Journal of Alloys and Compounds 695 (2017) 2930–2936

Contents lists available at ScienceDirect

Journal of Alloys and Compounds

journal homepage: http://www.elsevier.com/locate/jalcom

# High-sensitivity, high-selectivity, and fast-recovery-speed triethylamine sensor based on ZnO micropyramids prepared by molten salt growth method

Wenru Li, Hongyan Xu*, Ting Zhai, Huanqin Yu, Qi Xu, Xiaopan Song, Jieqiang Wang, Bingqiang Cao**

*School of Materials Science and Engineering, Laboratory of Inorganic Energy and Environment Materials, Shandong Provincial Key Laboratory of Preparation and Measurement, University of Jinan, Jinan 250022, Shandong, China*

ARTICLE INFO

*Article history:*
Received 7 November 2016
Received in revised form
23 November 2016
Accepted 26 November 2016
Available online 27 November 2016

*Keywords:*
ZnO micropyramids
Molten salt method
TEA sensing
Space-charge layer model

ABSTRACT

ZnO micropyramids had been successfully synthesized by an economical and environmental molten salt method (MSM). Compared with the reported works, we made a comprehensively and deeply sensing research for the ZnO micropyramids based triethylamine (TEA) sensors. The results of characterization reveal that the as-prepared ZnO crystallized sufficiently and have high purity. The sensors based on ZnO micropyramids have better TEA sensing performances, for instance higher response, better selectivity, and faster recovery speed than commercial ZnO. The response of ZnO micropyramids sensors can reach to 45 for 50 ppm of TEA. Moreover, the detection limit can also be as low as 2 ppm. These results indicate that the ZnO micropyramids synthesized by MSM are highly promising candidates for TEA gas detector. The space-charge layer model and the oxygen vacancies theory have also been proposed to interpret the gas sensing performance of ZnO micropyramids.

© 2016 Elsevier B.V. All rights reserved.

## 1. Introduction

Owing to the rapid development of industry, some environmental issues, especially air pollution, are the urgent tasks to be addressed in order to protect creatures on the earth and build a sustainable future. Triethylamine (TEA) is a common gas pollutant which generally secreted from the dead fish and seashells in our daily life [1,2]. As one of important industrial raw materials, TEA is also widely used for high energy fuels, preservatives, catalysts, and synthetic dyes [3]. However, the extremely toxic TEA easily causes great damage on human health, just like eyes irritations, skins burns, nausea, and even death. According to the regulation of Occupational Safety and Health Administration (OSHA), the threshold limit of TEA concentration in the air is 10 ppm on a volumetric basis (ppmV) [4–8]. To date, several methods have been adopted to realize effective detection for TEA, including gas/liquid/film chromatography, electrochemistry analysis, and colorimetric method [9–11]. Nevertheless, the wide application of those methods is limited by the complex and expensive equipment [12]. Thus, simple and economic detection of TEA, as well as favorable sensing properties, is still in great demand during our production and life [13].

Zinc oxide (ZnO), with band gap energy of 3.37 eV, has been already recognized as a very promising sensing material due to its controllable morphology, high electron mobility, and good chemical/thermal stability [14–18]. Many reports demonstrated that the ZnO-based sensors exhibited excellent sensing properties to not only small-molecule gases but also organic volatile compounds (VOCs) [19–23]. In the pursuit of high performances, the different morphologies of ZnO crystallites (nanorods [24], nanosheets [25], nanonails [26], and other special nanostructures) have been studied to realize better monitoring for gases. Thermal evaporation [27], chemical vapor deposition [28], metal-organic chemical vapor deposition [29], pulsed laser deposition [30], hydrothermal method [31], and other shape-controlled synthesis processes have been used to regulate the morphology of ZnO. Unfortunately, the large-scale application of those techniques is significantly affected by the precise instruments, complex production process, and energy intensive for now. Therefore, it is highly desirable to develop an

* Corresponding author.
** Corresponding author.
*E-mail addresses:* mse_xuhy@ujn.edu.cn (H. Xu), mse_caobq@ujn.edu.cn (B. Cao).

http://dx.doi.org/10.1016/j.jallcom.2016.11.380
0925-8388/© 2016 Elsevier B.V. All rights reserved.

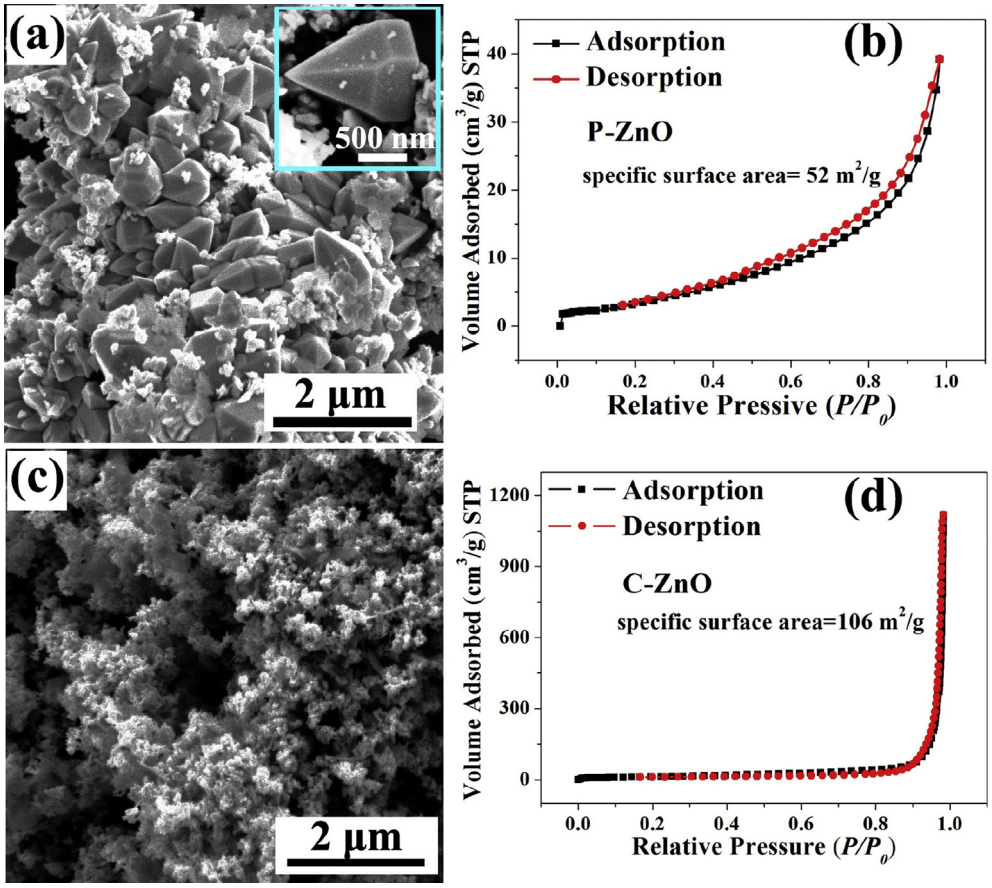


**Fig. 1.** (a) SEM image of P-ZnO with the best morphologies; (inset pattern) the SEM image of an individual P-ZnO crystallite; (b)nitrogen adsorption–desorption isotherm of P-ZnO; (c) SEM image of C-ZnO powder; (d) nitrogen adsorption–desorption isotherm of C-ZnO.

economical and environmental synthetic approach to produce highly sensitive TEA sensors.

Among various synthesis methods, molten salt method (MSM) has been applied into lithium ion battery, photo catalysis, gas sensors, and other fields for its easy-to-operate and low-cost [32–34]. For example, using MSM, Jin et al. [32] synthesized F-doped $Mn_3O_4$ nanobelts, which possessed an excellent reversible electrochemical lithium storage capacity. Xiang et al. [33] demonstrated a kind of CdS nanocrystals developed by MSM. The photo catalysis properties of synthesized nanocrystals were much better than commercial CdS powder under the irradiation of ultraviolet light source. In terms of gas sensors, Wang and co-workers [34] reported a $SnO_2$-based VOCs sensor fabricated with MSM that possesses fast response/recovery speed and low detection limit. Those results suggest that the MSM enables a high quality synthetic of semiconductors, which is widely accepted in many fields. We also notice that Xie et al. [35] prepared the pyramid-like ZnO crystallites in the same way, and investigated the influence of different crystal planes on photocatalysis and gas sensors [36]. However, they failed to make a comprehensively and deeply research about sensing performance in their works. In addition, the reports on fabricating ZnO micropyramids based TEA sensors are relatively rare. Therefore, it is still meaningful to investigate comprehensively TEA sensing properties on the basic of ZnO micropyramids made by MSM.

Here, we demonstrate the ZnO micropyramids TEA sensors with excellent sensing properties synthesized by an easily operating and low cost MSM. A relatively comprehensive TEA sensing was comparatively studied using commercial ZnO and as-prepared ZnO micropyramids. After comparison, both commercial ZnO and ZnO micropyramids showed a good stability for TEA sensing. However, the ZnO micropyramids exhibit higher response, better selectivity, and faster recovery speed than commercial ZnO. Further, the space-charge layer model and the oxygen vacancies theory are proposed to interpret the superior TEA sensing performance of ZnO micropyramids.

## 2. Experimental

### 2.1. Synthesis of ZnO micropyramids (P-ZnO)

The P-ZnO was synthesized by molten salt method (MSM) [34]. All of the chemical reagents were analytical graded and used without further purification. In the typical reaction, 0.219 g of $Zn(AC)_2 \bullet 2H_2O$ and 6.9 g of $LiNO_3$ were mixed together and ground sufficiently. After that, the mixture was transferred into an $Al_2O_3$ crucible and maintained at 400 °C for 30 min in the muffle furnace. When the crucible cooled down to room temperature spontaneously, the product was added into the deionized water. After stirring for 30 min, the white precipitates were collected by centrifugation, washed for several times with deionized water and absolute ethanol, and dried at 60 °C for 12 h in air. Then, the ZnO micropyramids powders were obtained. As a contrast sample, the commercial ZnO (C-ZnO) powders were available and needed no treatment.

### 2.2. Material characterizations

The morphology microstructures of two kinds of ZnO crystallites were measured by a field emission scanning electron

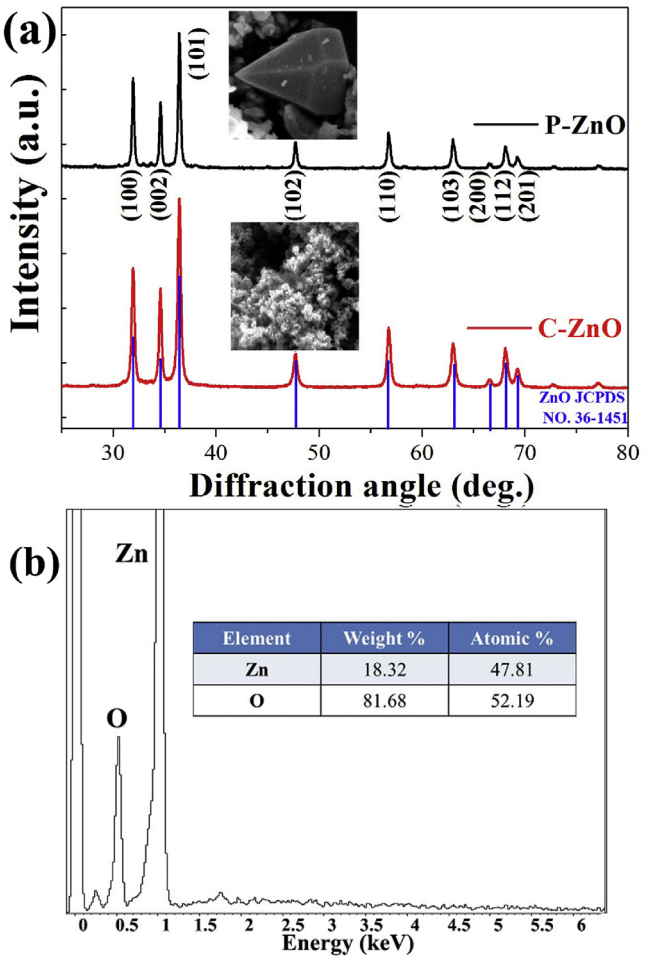


**Fig. 2.** (a) XRD patterns of P-ZnO and C-ZnO; (b) EDS spectrum of P-ZnO.

microscope (FESEM, FEI QUANTA FEG250) equipped with energy dispersive X-ray spectroscopy (EDS, INCA MAX-50) and a higher solution transmission electron microscope (HRTEM, JEM-2100F, JEOL). The phases of sensing materials were characterized by X-ray diffraction (XRD, Bruker D8 Advance diffractometer) using CuKal radiation ($\lambda = 0.15406$ nm) at 30 kV and 40 mA at a scanning rate of 2° at $2\theta$ $min^{-1}$ ranging from 20° to 80°.

### 2.3. Fabrication of gas sensors

When fabricating the sensors, the obtained samples were firstly mixed with distilled water to form slurry through milling, and then pasted onto a prefabricated alumina tube by a small brush to form a thick film. Gas sensing properties were tested by a gas-sensing characterization system (WS-30A, Wei Sheng Electronics Co., Ltd., China). Before the measurement, the sensors were aged at 350 °C for 24 h in air.

## 3. Results and discussion

### 3.1. Characterizations of ZnO crystallites

The SEM images and BET curves of ZnO samples are shown in Fig. 1. In Fig. 1 (a), most of the crystallites have complete and uniform pyramidal morphology with ~700 nm of basic size. An individual P-ZnO crystallite is shown in the inset pattern. Fig. 1(b) is the BET spectrum of P-ZnO crystallites, which provides more useful information about the specific surface area. The $N_2$ isotherm of P-ZnO is a type-IV isotherm with a large type H3 hysteresis loop [37]. The BET surface area of products is 53 $m^2/g$. Fig. 1(c) and (d) demonstrate that C-ZnO crystallites have quite small sizes and no regular morphology of grain with 106 $m^2/g$ of specific surface area. In theory, a large specific surface area is beneficial to the gas sensing of MOSs. However, the gas sensing properties of P-ZnO are much better than that of C-ZnO according the results of sensing test. The possible reasons would be proposed at last.

The crystallographic structures and phase purity of samples are confirmed by XRD (Fig. 2(a)). It can be found that all the characteristic peaks of two kinds of samples match well with the diffraction pattern of typical hexagonal wurtzite ZnO structure (JCPDS Card No. 36-1451) and no peaks are observed for other impurities. Furthermore, the P-ZnO was characterized by EDS. The EDS spectrum (Fig. 2(b)) clearly reveals that only the elements Zn and O are detected in the sample; no other impurity elements can be observed.

TEM, HRTEM, and SAED characterizations provide us with more useful information about the structural details. Fig. 3(a) shows the typical TEM image of an individual P-ZnO. The regular hexagonal profile of P-ZnO can be clearly observed in the inset pattern. As illustrated in Fig. 3(b), the lattice spacing is 0.247 nm, which represents $\{10\bar{1}1\}$ planes (the side surface of P-ZnO). The SAED pattern (Fig. 3(c)) indicates that the sample of P-ZnO is single crystallite. Learning from Fig. 3(d) and its inset pattern, we can know that the C-ZnO is irregular polycrystal particles with ~50 nm of the basic size, which coincides with the results of SEM just as shown in Fig. 1(c).

### 3.2. Sensing performance of ZnO based sensors

First of all, the gas sensing properties of the sensors were measured at different working temperature. Fig. 4(a) shows the response curves of the sensors to 50 ppm TEA at operating temperatures from 100 to 400 °C. As a function of temperature, the responses of the two sensors vary with operating temperature. Their optimal operating temperatures are both 300 °C, but the response of P-ZnO sensors can reach to 45 which is nearly two times higher than that of C-ZnO sensors (~20). When the operating temperature is higher than 300 °C, the gas sensing response decreased with the increasing of the temperature. This might due to the high operating temperature reduced the adsorption of gases on the surface of material [38]. The sensing performances comparison between the as-prepared P-ZnO sensors and literature results is summarized in Table 1. It is worth noting that the as-prepared P-ZnO sensors have much better gas sensing performances to TEA than that of the reported sensors, such as the lower detection limit and higher sensing response.

The responses of the sensors were examined by exposing the sensors to 100 ppm of TEA, alcohol, isopropanol, acetone, benzene, and p-xylene at 300 °C, respectively. As summarized in Fig. 4(b), the response of P-ZnO toward TEA can reach up to 43, which is nearly 4–10 times higher than that to other gases. This indicates that P-ZnO sensors have an excellent selectivity to TEA. Moreover, the selectivity of P-ZnO sensors is better than that of C-ZnO sensors. The different responses to target gases may due to the different main molecular bonds, and the detail has been discussed by the previous works [44,45]. The main bond energies of target gases, for example, C–N (TEA), C–C (isopropanol), O–H (ethanol), C=C (benzene), and C=O (acetone), are 307, 345, 458.8, 610.3, and 798.9 kJ/mol, respectively. The relatively low C–N bond energy of TEA molecules is expected to result in the high response.

The dynamic-sensing responses of the two kinds of sensors were also investigated for detecting TEA at 300 °C. In Fig. 5(a), the

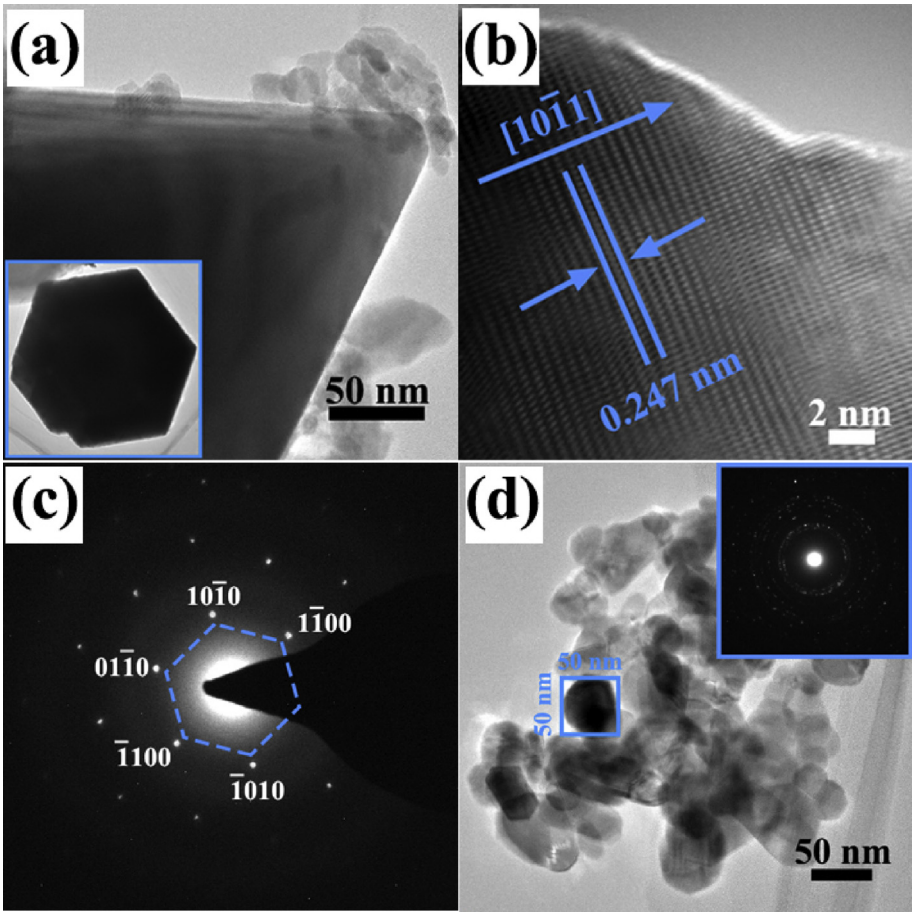


**Fig. 3.** (a) TEM image of P-ZnO; corresponding (b) HRTEM and(c) SAED images of an individual P-ZnO; (d) TEM image of C-ZnO, the inset pattern is the corresponding SAED image of the C-ZnO crystallites.

dynamic-sensing response versus time of two sensors is demonstrated, with the TEA concentration varying from 2 to 500 ppm. The response of P-ZnO sensor keeps growing with increasing TEA concentration. While for C-ZnO sensor, the response has no apparent variation after 100 ppm, which indicting that the detection upper limit of C-ZnO is much lower than that of P-ZnO sensor. The tendency of responses can be observed more clearly in the inset pattern. Furthermore, when TEA concentration is as low as 2 ppm, P-ZnO sensors show a better response about 5, which indicates a relatively low detection limit. And in our work, the responses of two kinds of sensors exhibit good linear relationship with the concentration in a logarithm scale, just as shown in Fig. 5(b).

The repeatability is another important sensing index for the actual application of gas sensors. Fig. 6 shows typical response profiles of two kinds of sensors to 50 ppm TEA at 300 °C. Consistent sensing responses with excellent recovery characteristics can be observed after running 5 cycles, which illustrates the good repeatability of our sensors.

A fast response-recovery speed is essential for gas sensors. The response-recovery time is defined as the time taken by the sensor to achieve 90% of the total resistance change in the case of gas adsorption ($T_a$) and desorption ($T_b$), respectively. As demonstrated in Fig. 7, both two sensors show fast response speed upon exposure to the TEA gas, which is 10 s for P-ZnO sensors and 11 s for C-ZnO sensors, respectively. However, the P-ZnO sensors need shorter time to recover than C-ZnO sensors after the gas was removed. The $T_b$ of P-ZnO sensor is 48 s, which is nearly 32 s less than that of C-ZnO sensor. Moreover, the recovery time of the as-prepared P-ZnO sensors is obviously shorter than reported TEA sensors. For example, in 2015, Sui et al. [3] synthesized flower-like α-$MoO_3$ by solvothermal route, toward 0.5 ppm and 100 ppm of TEA, the recovery times are 161 and 1283 s, respectively. In 2016, Liu et al. [46] prepared a light irradiation enhanced ZnO/$ZnFe_2O_4$ sensors for TEA gas detection. Toward different concentrations of TEA, the response times are all about 100 s. Compared with the above mentioned, our sensors have more rapid recovery speed.

### 3.3. Mechanism discussion

The gas sensing mechanism of n-type MOSs based sensors such as ZnO which accepted most commonly is the space-charge layer model and this mechanism mainly involves the gas adsorption, charge transfer, and desorption process [47–49]. For MOSs based gas sensors, the change of sensor resistance is caused by the transfer of free charge carriers (electrons or holes) from/to the semiconductor to/from adsorbed oxygen [50]. As demonstrated in Fig. 8(a), when the P-ZnO sensors were exposed to air at a relative high temperature, oxygen molecules in the air would be adsorbed on the ZnO surface and ionized to $O^{\delta-}$ by capturing free electrons from the conduction band of ZnO, which promotes the formation of depletion layer with high resistance state ($R_a$) on the surface of P-ZnO. Once the P-ZnO sensors were exposed to reducing TEA gas, the

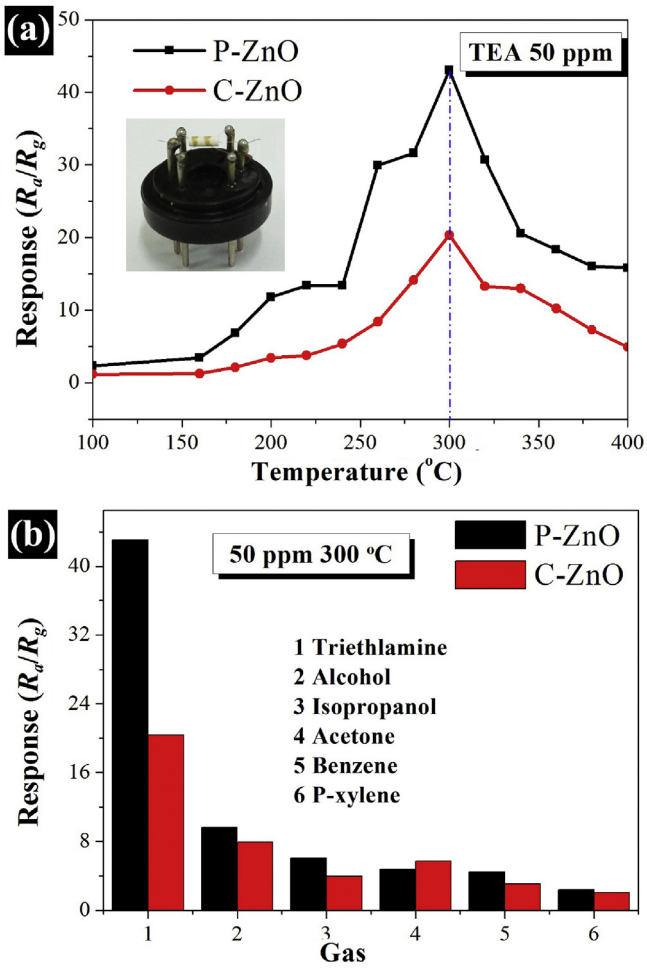


**Fig. 4.** (a) Curves of gas sensitivity versus working temperature to 50 ppm TEA gas; (inset pattern) gas sensor fixed on an electronic bracket; (b) the selectivity of two kinds of sensors for different target gases with the same concentration.

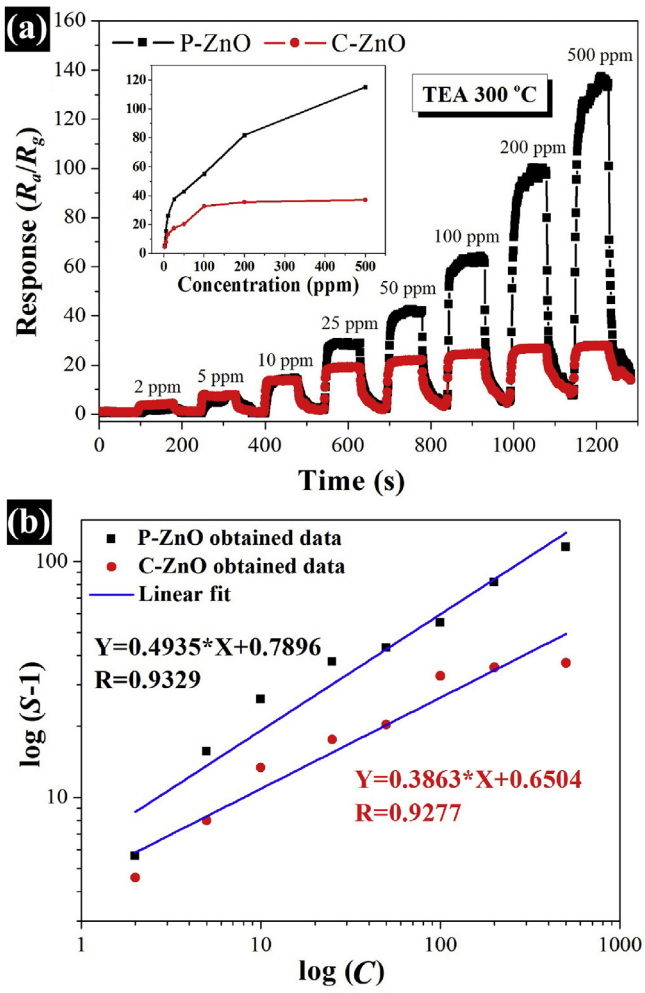


**Fig. 5.** (a) Responses of two kinds of sensors to TEA of different concentration; (inset pattern) corresponding relationship between response and concentration; (b) The log(*S*-1) versus log(*C*) plot of two kinds of ZnO sensors for TEA gas and the corresponding linearly fitted results.

TEA molecules would react with the oxygen ions on the surface, with the trapped electrons being released back to the conduction band of the ZnO. The reaction between TEA and surface oxygen species can be simply described as [51,52].

$$(C_2H_5)_3N + O^{\delta-} \leftrightarrow CO_2 + H_2O + NO_2 + e^-$$

This process increases the electron concentration, and ultimately decreases in resistance state ($R_g$) of the sensors. The sensor response is defined as follow: $S = R_a/R_g$. The corresponding change of energy band diagram (Fig. 8(b)) demonstrates the same progress. Before reacting with TEA molecules, a number of electrons transfer to the vicinity of crystal surface. This process is described in the energy bands representation as an upward band bending just as shown in Fig. 8(b) left. After reacting with the gases molecules, like Fig. 8(b) right described, the concentration of surface negative charge would decrease, which relaxed the bending degree of the energy band. As a result, the resistance of material changes along with the variation of energy band.

Theoretically, for pure ZnO gas sensing materials, the larger its surface area is, the higher the gas sensitivity would be [53]. In our work, the specific surface area of C-ZnO crystallites is two times larger than that of P-ZnO crystallites according to the results of

**Table 1**
TEA sensing properties of ZnO micropyramids and other reported oxide semiconductor gas sensors working under different operating temperatures.

| Material | Concentration (ppm) | Operating temperature (°C) | Response ($R_a/R_g$) | References |
|---|---|---|---|---|
| ZnO micropyramids | 50 | 300 | 45 | Our work |
| ZnO nanorods | 500 | 150 | 300 | [39] |
| ZnO film | 50 | 40 | 3 | [40] |
| Porous ZnO foam | 90 (ppb) | 350 | 1.4 | [41] |
| $SnO_2$ nanorods | 100 | 350 | 140 | [34] |
| α-$MoO_3$ Flower | 100 | 250 | 416 | [3] |
| $V_2O_5$ hollow spheres | 100 | 370 | 7.3 | [42] |
| $Cr_2O_3$ microspheres | 50 | 170 | 17 | [43] |

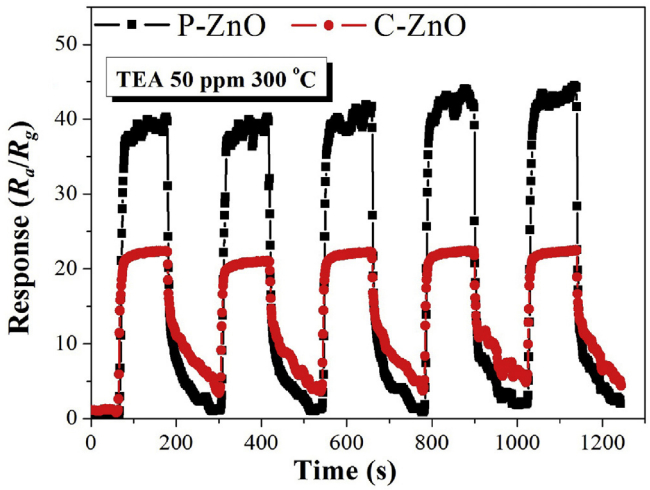


**Fig. 6.** The device repeatability of the two kinds of sensors to 50 ppm TEA at 300 °C.

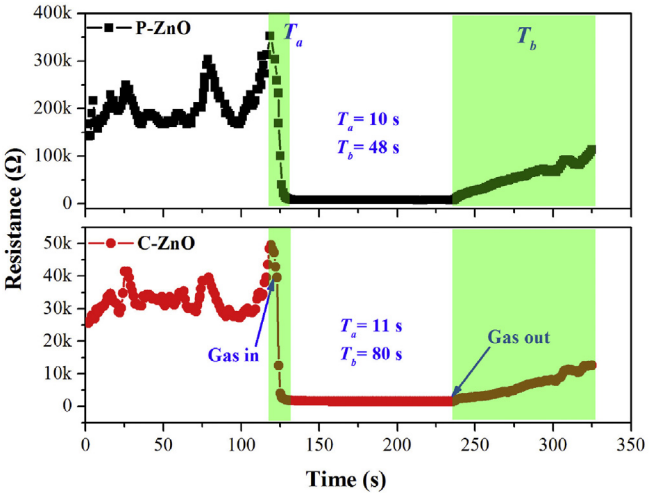


**Fig. 7.** The response-recovery curve of the two sensors to 50 ppm TEA at 300 °C.

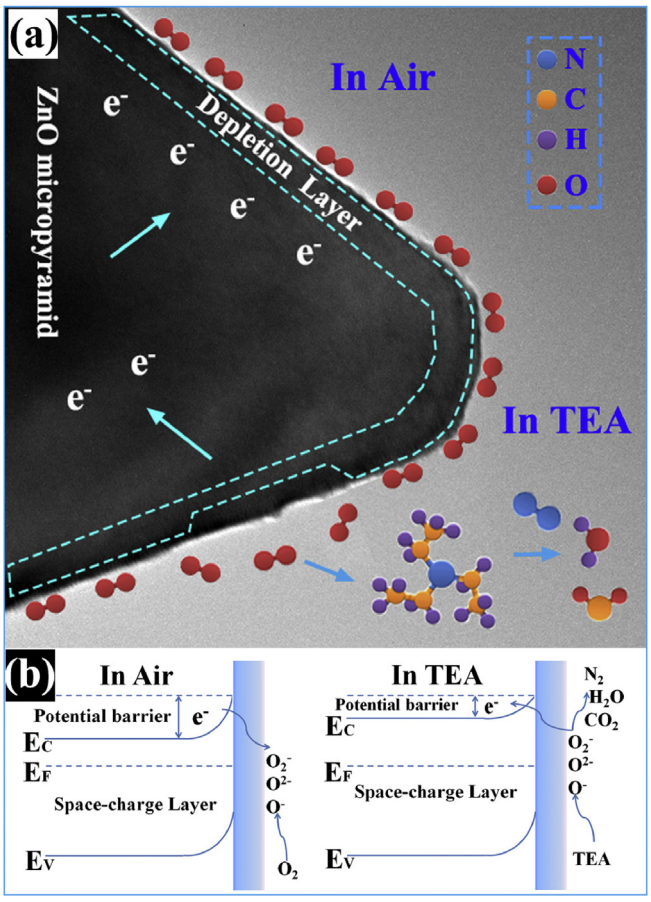


**Fig. 8.** (a) Schematic model of the P-ZnO sensors exposing to air and TEA gas, respectively; (b) the corresponding change of energy band diagram of P-ZnO.

BET. Contrary to the general conclusion, P-ZnO sensors reveal better sensing properties in the aspects of sensitivity, selectivity, and recovery speed than C-ZnO sensors. The possible reasons are presented as follows: Primarily, the existence of oxygen vacancies will greatly affect the performance of gas sensors. Jiang et al. [54] found that P-ZnO crystallites exhibit a lot of oxygen vacancies on their planes. And the presence of the oxygen vacancies could enhance gas sensing of ZnO-based sensors [55–58]. Oxygen vacancies act as the electron donor which providing electrons to the conduction band of P-ZnO and absorbing more oxygen species [59]. By the way, the loose structure of C-ZnO may trap the escape of gas molecules, which led to a slow recovery speed. In another word, the regular morphology of P-ZnO relatively contributes to desorption of gases.

## 4. Conclusions

In summary, we successfully synthesized P-ZnO crystallites by molten salt method. The as-prepared P-ZnO sensors exhibit higher response (5) at a low concentration (2 ppm) of TEA, good selectivity to TEA, and short response-recovery times (about 10 s, 48 s, respectively), which are much better than those of C-ZnO sensors. The gas sensing mechanism of P-ZnO was also discussed in detail. It is worth mentioning that, the molten salt method is a simple and effective way to produce MOSs with special structures and could be applied into actual production.

## Acknowledgements

This work is supported by National Natural Science Foundation of China (NSFC, No. 60906008), Shan-dong Provincial Science Foundation (No. ZR2014JL045) and Science Foundation of University of Jinan (No. XKY1504).

## References

[1] W.H. Zhang, W.D. Zhang, Fabrication of $SnO_2$-ZnO nanocomposite sensor for selective sensing of trimethylamine and the freshness of fishes, Sens. Actuators B 134 (2008) 403–408.
[2] Q. Xu, D.X. Ju, Z.C. Zhang, S. Yuan, J. Zhang, H.Y. Xu, B.Q. Cao, Near room-temperature triethylamine sensor constructed with CuO/ZnO P-N heterostructural nanorods directly on flat electrode, Sens. Actuators B 225 (2016) 16–23.
[3] L.L. Sui, Y.M. Xu, X.F. Zhang, X.L. Cheng, S. Gao, H. Zhao, Z. Cai, L.H. Huo, Construction of three-dimensional flower-like α-$MoO_3$ with hierarchical structure for highly selective triethylamine sensor, Sens. Actuators B 208 (2015) 406–414.
[4] B. Gandu, K. Sandhya, A.G. Rao, Y.V. Swamy, Gas phase bio-filter for the removal of triethylamine (TEA) from air: microbial diversity analysis with reference to design parameters, Bioresour. Technol. 139 (2013) 155–160.
[5] L. Xu, H.J. Song, J. Hu, Y. Lv, K.L. Xu, A cataluminescence gas sensor for triethylamine based on nanosized $LaF_3$–$CeO_2$, Sens. Actuators B 169 (2012) 261–266.

[6] Y.C. Chien, S.N. Uang, C.T. Kuo, T.S. Shih, J.F. Jen, Analytical method for monitoring airborne trimethylamine using solid phase micro-extraction and gas chromatography-flame ionization detection, Anal. Chim. Acta 419 (2000) 73–79.

[7] M. Asif, J.E. Szulejko, K.H. Kim, Determination of methylamine, dimethylamine, and trimethylamine in air by high-performance Liquid chromatography with derivatization using 9-fluorenylmethylchloroformate, Anal. Methods 6 (2014) 5697–5707.

[8] Y.H. Kim, K.H. Kim, An accurate and reliable analysis of trimethylamine using thermal desorption and gas chromatography–time of flight mass spectrometry, Anal. Chim. Acta 780 (2013) 46–54.

[9] W.H. Zhang, W.D. Zhang, Fabrication of $SnO_2$–ZnO nanocomposite sensor for selective sensing of trimethylamine and the freshness of fishes, Sens. Actuators B Chem. 134 (2008) 403–408.

[10] W.M. Moore, R.J. Edwards, L.T. Bavda, An improved capillary gas chromatography method for triethylamine: application to sarafloxacin hydrochloride and GnRH residual solvents testing, Anal. Lett. 32 (1999) 2603–2612.

[11] J.F. Haskin, G.W. Warren, L.J. Priestley, Gas chromatography determination of constituents in the study of azeotropes, Anal. Chem. 30 (1958) 217–219.

[12] D.X. Ju, H.Y. Xu, Z.W. Qiu, Z.C. Zhang, Q. Xu, J. Zhang, J.Q. Wang, B.Q. Cao, Near room temperature, fast-response, and highly sensitive triethylamine sensor assembled with Au-Loaded ZnO/$SnO_2$ core-shell nanorods on flat alumina substrates, ACS Appl. Mater. Interfaces 7 (2015) 19163–19171.

[13] E. Filippo, D. Mannob, A. Buccolieri, A. Serra, Green synthesis of sucralose-capped silver nanoparticles for fast colorimetric triethylamine detection, Sens. Actuators B Chem. 178 (2013) 1–9.

[14] Z. Qin, Y.H. Huang, J.J. Qi, H. Feng, L.J. Su, Y. Zhang, Facile synthesis and photoelectrochemical performance of the bush-like ZnO nanosheets film, Solid State Sci. 14 (2012) 155–158.

[15] X. Han, Y. Sun, Z.Y. Feng, G.C. Zhang, Z.C. Chen, J.H. Zhan, Au-deposited porous single-crystalline ZnO nanoplates for gas sensing detection of total volatile organic compounds, RSC Adv. 6 (2016) 37750–37756.

[16] D.X. Ju, H.Y. Xu, J. Zhang, J. Guo, B.Q. Cao, Highly sensitive and selective triethylamine-sensing properties of nanosheets directly grown on ceramic tube by forming NiO/ZnO PN heterojunction, Sens. Actuators B 200 (2014) 288–296.

[17] Z.P. Fu, Z. Wang, B.F. Yang, Y.L. Yang, H.W. Yan, L.S. Xia, Shape-control of nano-ZnO by changing the solvent, Mater. Lett. 61 (2007) 4832–4835.

[18] J. Zhang, X.H. Liu, G. Neri, N. Pinna, Nanostructured materials for room-temperature gas sensors, Adv. Mater 28 (2016) 795–831.

[19] J. Kim, K. Yong, Mechanism study of ZnO nanorod-bundle sensors for $H_2S$ gas sensing, J. Phys. Chem. C 115 (2011) 7218–7224.

[20] F.T. Liu, S.F. Gao, S.K. Pei, S.C. Tseng, C.J. Liu, ZnO nanorod gas sensor for $NO_2$ detection, J. Taiwan Inst. Chem. Eng. 40 (2009) 528–532.

[21] N.D. Khoang, H.S. Hong, D.D. Trung, N.V. Duy, N.D. Hoa, D.D. Thinh, N.V. Hieu, On-chip growth of wafer-scale planar-type ZnO nanorod sensors for effective detection of CO gas, Sens. Actuators B 181 (2013) 529–536.

[22] S.R. Wang, J.X. Zhang, J.D. Yang, X.L. Gao, H.X. Zhang, Y.S. Wang, Z.Y. Zhu, Spinel $ZnFe_2O_4$ nanoparticle-decorated rod-like ZnO nanoheterostructures for enhanced gas sensing performances, RSC Adv. 5 (2015) 10048–10057.

[23] S.M. Wang, P. Wang, Z.F. Li, C.H. Xiao, B.X. Xiao, R. Zhao, T.Y. Yang, M.Z. Zhang, Highly enhanced methanol gas sensing properties by $Pd_{0.5}Pd_3O_4$ nanoparticle loaded ZnO hierarchical structures, RSC Adv. 4 (2014) 35375–35382.

[24] J. Chang, E. Waclawik, Facet-controlled self-assembly of ZnO nanocrystals by non-hydrolytic aminolysis and their photo degradation activities, CrystEngComm 14 (2012) 4041–4048.

[25] P.K. Samanta, S.K. Patra, P.R. Chaudhuri, Violet emission from flower-like bundle of ZnO nanosheets, Phys. E 41 (2009) 664–667.

[26] X.B. Song, Y.H. Zhang, J. Zheng, X.G. Li, Low-temperature synthesis of ZnO nanonails, J. Phys. Chem. Solids 68 (2007) 1681–1684.

[27] M.S. Kim, G.H. Lee, Synthesis of ZnO crystals with octahedral morphology through thermal evaporation technique in air, Mater. Trans. 55 (2014) 690–692.

[28] A. Menzel, K. Komin, Y. Yang, F. Güder, V. Trouillet, P. Werner, M. Zacharias, Ultra-long zinc oxide nanowires and boron doping based on ionic liquid assisted thermal chemical vapor deposition growth, Nanoscale 7 (2014) 92–97.

[29] J.L. Yang, S.J. An, W.I. Park, G.C. Yi, W. Choi, Photocatalysis using ZnO thin films and nanoneedles grown by metal–organic chemical vapor deposition, Adv. Mater 16 (2004) 1661–1664.

[30] Y. Sun, G.M. Fuge, M.N.R. Ashfold, Growth of aligned ZnO nanorod arrays by catalyst-free pulsed laser deposition methods, Chem. Phys. Lett. 396 (2004) 21–26.

[31] J. Guo, J. Zhang, M. Zhu, D.X. Ju, H.Y. Xu, B.Q. Cao, High-performance gas sensor based on ZnO nanowires functionalized by Au nanoparticles, Sens. Actuators B 199 (2014) 339–345.

[32] R.C. Jin, H. Liu, Y.S.I. Guan, J.H. Zhou, G.H. Li, Molten salt synthesis of fluorine-doped $Mn_3O_4$ nanobelts as anode materials for Li-ion batteries, Cryst. Eng. Comm. 17 (2015) 7717–7722.

[33] D.H. Xiang, Y.B. Zhu, C.J. Cai, Z.J. He, Z.S. Liu, D.G. Yin, J. Luo, A new simple synthesis of CdS nano-particles by composite-molten-salt method and their high photocatalytic degradation activity, Phys. E 44 (2011) 733–737.

[34] D. Wang, X.F. Chu, M.L. Gong, Gas-sensing properties of sensors based on single-crystalline $SnO_2$ nanorods prepared by a simple molten-salt method, Sens. Actuators B 117 (2006) 183–187.

[35] X. Zhou, Z.X. Xie, Z.Y. Jiang, Q. Kuang, S.H. Zhang, T. Xu, R.B. Huang, L.S. Zheng, Formation of ZnO hexagonal micro-pyramids: a successful control of the exposed polar surfaces with the assistance of an ionic liquid, Chem. Commun. 44 (2005) 5572–5574.

[36] X.G. Han, H.Z. He, Q. Kuang, X. Zhou, X.H. Zhang, T. Xu, Z.X. Xie, L.S. Zheng, Controlling morphologies and tuning the related properties of nano/micro-structured ZnO crystallites, J. Phys. Chem. C 113 (2009) 584–589.

[37] Z.H. Jing, J.H. Zhan, Fabrication and gas-sensing properties of porous ZnO nanoplates, Adv. Mater 20 (2008) 4547–4551.

[38] X.F. Chu, T.Y. Chen, W.B. Zhang, B.Q. Zheng, H.F. Shui, Investigation on formaldehyde gas sensor with ZnO thick film prepared through microwave heating method, Sens. Actuators B 142 (2009) 49–54.

[39] Y.Z. Lv, C.R. Li, L. Guo, F.C. Wang, Y. Xu, X.F. Chu, Triethylamine gas sensor based on ZnO nanorods prepared by a simple solution route, Sens. Actuators B 141 (2009) 85–88.

[40] S.H. Park, J.Y. Ryu, H.H. Choi, T.H. Kwon, Zinc oxide thin film doped with $Al_2O_3$, $TiO_2$ and $V_2O_5$ as sensitive sensor for trimethylamine gas, Sens. Actuators B 46 (1998) 75–79.

[41] J.L. Wang, C.J. Pei, L.J. Cheng, W.P. Wan, Q. Zhao, H.Q. Yang, S.Z. Liu, Responses of three-dimensional porous ZnO foam structures to the trace level of triethylamine and ethanol, Sens. Actuators B 223 (2016) 650–657.

[42] M.Z. Wu, X.F. Zhang, S. Gao, X.L. Cheng, Z.M. Rong, Y.M. Xu, H. Zhao, L.H. Huo, Construction of monodisperse vanadium pentoxide hollow spheres via a facile route and triethylamine sensing property, Cryst. Eng. Comm. 15 (2013) 10123–10131.

[43] J. Cao, Y.M. Xu, L.L. Sui, X.F. Zhang, S. Gao, X.L. Cheng, H. Zhao, L.H. Huo, Highly selective low-temperature triethylamine sensor based on Ag/$Cr_2O_3$ mesoporous microspheres, Sens. Actuators B 220 (2015) 910–918.

[44] L.X. Zhang, J.H. Zhao, H.Q. Lu, L. Li, J.F. Zheng, J. Zhang, H. Li, Z.P. Zhu, Highly sensitive and selective dimethylamine sensors based on hierarchical ZnO architectures composed of nanorods and nanosheet-assembled microspheres, Sens. Actuators B 171–172 (2012) 1101–1109.

[45] H.Y. Xu, D.X. Ju, W.R. Li, H.B. Gong, J. Zhang, J.Q. Wang, B.Q. Cao, Low-working-temperature, fast-response-speed $NO_2$ sensor with nanoporous-SnO 2/polyaniline double-layered film, Sens. Actuators B 224 (2016) 654–660.

[46] S.R. Liu, M.Y. Guan, X.Z. Li, Y. Guo, Light irradiation enhanced triethylamine gas sensing materials based on ZnO/$ZnFe_2O_4$ composites, Sens. Actuators B 236 (2016) 350–357.

[47] H.Y. Xu, D.X. Ju, W.R. Li, J. Zhang, J.Q. Wang, B.Q. Cao, Superior triethylamine-sensing properties based on $TiO_2$/$SnO_2$ n–n heterojunction nanosheets directly grown on ceramic tubes, Sens. Actuators B 228 (2016) 634–642.

[48] E. Filippo, D. Mannob, A. Buccolieri, A. Serra, Green synthesis of sucralose-capped silver nanoparticles for fast colorimetric triethylamine detection, Sens. Actuators B 178 (2013) 1–9.

[49] H.C. Chiu, C.S. Yeh, Hydrothermal synthesis of $SnO_2$ nanoparticles and their gas-sensing of alcohol, J. Phys. Chem. C 111 (2007) 7256–7259.

[50] N. Barsan, C. Simion, T. Heine, S. Pokhrel, U. Weimar, Modeling of sensing and transduction for p-type semiconducting metal oxide based gas sensors, J. Electroceram. 25 (2010) 11–19.

[51] J. Wang, L. Yu, H. Wang, S. Ruan, J. Li, F. Wu, Preparation and triethylamine sensing properties of Ce-doped $In_2O_3$ nanofibers, Acta. Phys. Chim. Sin. 26 (2010) 3101–3105.

[52] Y. Takao, M. Nakanishi, T. Kawaguchi, Y. Shimizu, M. Egashira, Semiconductor dimethylamine gas sensors with high sensitivity and selectivity, Sens. Actuators B 24–25 (1995) 375–379.

[53] J. Xu, Q. Pan, Y. Shun, Z. Tian, Grain size control and gas sensing properties of ZnO gas sensor, Sens. Actuators B 66 (2000) 277–279.

[54] Z.Y. Jiang, Q. Kuang, Z.X. Xie, L.S. Zheng, Syntheses and properties of micro/nanostructured crystallites with high-energy surfaces, Adv. Funct. Mater 20 (2010) 3634–3645.

[55] Y.R. Wang, B. Liu, S.H. Xiao, X.H. Wang, L.M. Sun, H. Li, W.Y. Xie, Q.H. Li, Q. Zhang, T.H. Wang, Low-temperature $H_2S$ detection with hierarchical Cr-Doped $WO_3$ microspheres, ACS Appl. Mater. Interfaces 8 (2016) 9674–9683.

[56] D.E. Motaung, G.H. Mhlongo, I. Kortidis, S.S. Nkosi, G.F. Malgas, B.W. Mwakikunga, S.S. Ray, G. Kiriakidis, Structural and optical properties of ZnO nanostructures grown by aerosol spray pyrolysis: candidates for room temperature methane and hydrogen gas sensing, Appl. Surf. Sci. 279 (2013) 142–149.

[57] W. Kim, M. Choi, K. Yong, Generation of oxygen vacancies in ZnO nanorods/films and their effects on gas sensing properties, Sens. Actuators B 209 (2015) 989–996.

[58] L.W. Wang, Y.F. Kang, X.H. Liu, S.M. Zhang, W.P. Huang, S.R. Wang, ZnO nanorod gas sensor for ethanol detection, Sens. Actuators B 162 (2012) 237–243.

[59] H. Huang, O.K. Tan, Y.C. Lee, T.D. Tran, M.S. Tse, X. Yao, Semiconductor gas sensor based on tin oxide nanorods prepared by plasma-enhanced chemical vapor deposition with postplasma treatment, Appl. Phys. Lett. 87 (2005) 163123–163123-3.